Available online at www.sciencedirect.com
SCIENCE DIRECT®
International Journal of Heat and Mass Transfer 48 (2005) 501–509
International Journal of HEAT and MASS TRANSFER
www.elsevier.com/locate/ijhmt

Numerical investigation of ultrashort laser damage in semiconductors

J.K. Chen [a,*], D.Y. Tzou [b], J.E. Beraun [a]

[a] *Laser Effects Research Branch, Directed Energy Directorate, Air Force Research Laboratory, 3550 Aberdeen Avenue SE, Kirtland AFB, NM 87117-5776, USA*
[b] *Department of Mechanical and Aerospace Engineering, University of Missouri—Columbia, Columbia, MO 65211, USA*

Received 26 February 2004; received in revised form 10 September 2004
Available online 6 November 2004

Abstract

A complete self-consistent model for transport dynamics in semiconductors caused by ultrashort-pulse laser heating is presented based on the relaxation-time approximation of the Boltzmann equation. Carrier–lattice nonequilibrium interactions are simulated to obtain the temporal and spatial evolution of the carrier density and temperature as well as the lattice temperature. It is shown that the calculated damage threshold based on the carrier density criterion agrees fairly well with the experimental data for both Si and Ge semiconductors, especially for sub-picosecond pulses. It is also found that one-photon absorption and Auger recombination are the two critical factors that influence the electron–hole carrier generation.
© 2004 Elsevier Ltd. All rights reserved.

1. Introduction

Laser annealing process of semiconductor materials has been the subject of a great number of investigations since late 1970s [1]. The issue that attracts the most attention is the nature of the induced phase transition that accompanies pulse laser annealing and renders a disordered solid into a near-perfect crystal. For pulse durations longer than the carrier–lattice energy relaxation time (a few picoseconds), it has generally been accepted that the solid–liquid phase transition by high enough laser fluences is a rapid thermal process [2], which results from the fast energy exchange between the optically excited electrons and the lattice. On the other hand, experiments with femtosecond (fs) laser pulses of high fluences have demonstrated ultrafast phase transformation on a subpicosecond time scale [3–7]. The mechanism of this ultrafast phase transformation differs from the above thermal melting. Under ultrashort-pulse laser excitation high density (10^{21}–$10^{22}\,cm^{-3}$) and high temperature ($\geqslant 1000\,K$) electrons could be photoexcited from valence band into the conduction band. As a result of a large number of covalent bonds destroyed, the lattice experiences a dramatic reduction in its shear force and undergoes a plasma-mediated phase transition [8]. Since the lattice instability occurs prior to the significant heating of the phonon subsystem, this damage is referred to as a non-thermal melting.

Although the kinetics of high-density plasma generated in a semiconductor by ultrashort laser pulses have theoretically been investigated in many papers, a

* Corresponding author. Tel.: +1 505 853 3184; fax: +1 505 846 1625.

0017-9310/$ - see front matter © 2004 Elsevier Ltd. All rights reserved.
doi:10.1016/j.ijheatmasstransfer.2004.09.015

Nomenclature

b	radius where I is e^{-1} times of that at the laser spot center
C	heat capacity
D	ambipolar diffusion coefficient
E	energy
e	constant (=2.718)
F	Fermi–Dirac integral
H	ratio of two Fermi–Dirac integrals
h	Planck's constant
$\hbar$	$h/2\pi$
L	sample thickness
I	laser intensity
I_0	transmitted laser intensity at the incident surface
$\bar{j}$	carrier current vector
k_B	Boltzmann constant
m^*	effective mass
N	effective density of states
n	number density of carriers
Q	heat flux
q	charge of an electron
R	surface reflectivity
r	radius
S	Seeback coefficient
T	temperature (K)
t	time
t_p	pulse duration defined as the full width at the half maximum
U	total energy density in carrier pairs
$\overline{W}$	ambipolar energy current vector
$\bar{w}$	energy current vector
$\bar{x}$	position vector
z	direction of laser beam propagation

Greek symbols

α	one-photon absorption coefficient
β	two-photon absorption coefficient
δ	optical penetration depth
Φ	laser energy
ϕ	laser fluence
Γ	Gamma function
γ	Auger recombination coefficient
η	reduced Fermi level
φ	quasi-Fermi level
κ	thermal conductivity
μ	mobility of carriers
v	radiation of frequency
π	Peltier coefficient
Θ	free-carrier absorption cross-section
θ	impact ionization coefficient
σ	electrical conductivity
τ	relaxation time
ω	constant (=$4\ln 2$)
ξ, ζ	order of Fermi–Dirac integral

Subscripts and superscripts

C	conduction band
c	carrier
e	electron
e–h	electron–hole pair
f	onset of the damage
g	band gap
h	hole
l	lattice (phonon)
0	Maxwell–Boltmann distribution
V	valence band

calculation of melting or more generally of damage threshold has not been done consistently so far due to a lack of the knowledge of accurate material properties and the true criterion for melting [9]. There are two methods used in the evaluation of the damage threshold for semiconductors. One approach employs a single rate equation to evaluate the electron density in the conduction band [10]. Melting is assumed when the calculated electron density exceeds a critical density. The other approach uses a self-consistent model to simulate the electron density in the conduction band, the carrier temperature, and the phonon temperature [9]. The latter allows the determination of melting damage based on the electron density or the lattice temperature. The agreement between the theoretical and experimental values reported for Si [9] is somewhat satisfying for laser pulse durations shorter than two picoseconds (ps). The deviation for the longer pulses was attributed to the negligence of the diffusion terms in the self-consistent model.

In this paper, a complete self-consistent model that describes the electron–hole carrier density and current, the ambipolar energy current, and the carrier and lattice temperature is presented based on the relaxation-time approximation of the Boltzmann equation [11]. Temperature-dependent multi-photon and free-carrier absorptions are considered. The coupled set of nonlinear equations is solved with a finite difference method for the carrier density and temperature as well as the lattice temperature. Whether the diffusion effects impact the carrier density prediction is investigated. A rate equation that models the carrier density along is also reduced from the complete self-consistent model. The theoretical melting thresholds are compared with the experimental data for Si and Ge semiconductors [9].

2. Ultrafast transport dynamics in semiconductors

When a semiconductor is excited with a short laser pulse, electrons absorb the photon energy and transit from the valence to the conduction band via single- and/or multi-photon absorption, depending on the photon energy ($h\nu$) and the band-gap energy (E_g). This interband transition of the electrons creates holes in the valence band. As electrons and holes undergo temporal and spatial evolution, a part of them recombine via the three-body Auger process. In the meantime, new electron–hole pairs are generated via impact ionization. The excess energy of the created electron–hole pairs, $h\nu$–E_g and/or $2h\nu$–E_g, is the kinetic energy that leads to elevated carrier temperatures. The carriers then thermalize into the Fermi–Dirac distribution via carrier–carrier collisions on a $<10^{-13}$ s time scale. The distribution functions for the electrons and holes can possess different quasi-Fermi levels but have a common temperature ($T_e = T_h$). Meanwhile, a thermalization between the carriers and the phonons proceeds, and the thermal equilibrium state will be established.

To model the transport process of a large number of hot electrons, holes, and phonons in a semiconductor, the formalism must be based on the principle of statistical mechanics. The non-equilibrium states can thus be represented with local values of the statistical parameters. The formulation of ultrafast transport dynamics in semiconductors presented below follows Drabble and Goldsmid [11] and van Driel [12]. From the relaxation-time approximation of the Boltzmann equation, one has the electrical and energy current of the carriers

$$\bar{j}_c = \frac{\sigma_c}{q}\nabla\varphi_c - \sigma_c S_c \nabla T_c \tag{1}$$

$$\bar{w}_c = \left(\pi_c - \frac{\varphi_c}{q}\right)\bar{j}_c - \kappa_c \nabla T_c \tag{2}$$

The above four transport parameters, σ_c, S_c, π_c and κ_c, are given by

$$\sigma_c = q n_c \mu_c^0 H_{1/2}^0(\eta_c) \tag{3}$$

$$S_c = -\frac{k_B}{q_c}\left[\eta_c - 2H_0^1(\eta_c)\right] \tag{4}$$

$$\pi_c = T_c S_c \tag{5}$$

$$\kappa_c = \frac{k_B^2 \sigma_c T_c}{q^2}\left[6H_0^2(\eta_c) - 4H_0^1(\eta_c)^2\right] \tag{6}$$

where q_c equals $-q$ for electrons and $+q$ for holes, and $H_\zeta^\xi(\eta_c) = F_\xi(\eta_c)/F_\zeta(\eta_c)$ with $F_\xi(\eta_c)$ denoting the Fermi–Dirac integral of order ξ

$$F_\xi(\eta_c) = \frac{1}{\Gamma(\xi+1)}\int_0^\infty \frac{x^\xi}{1+\exp(x-\eta_c)}\mathrm{d}x \tag{7}$$

The reduced Fermi level η_c is respectively defined as

$$\eta_e = \frac{\varphi_e - E_C}{kT_e} \quad \text{and} \quad \eta_h = \frac{E_V - \varphi_h}{kT_h} \tag{8}$$

The local carrier density (n_c) is obtained by integrating over the microscopic quasi-equilibrium distribution functions [13]

$$n_c = 2\left[\frac{m_c^* k_B T_c}{2\pi\hbar^2}\right]^{3/2} F_{1/2}(\eta_c) \tag{9}$$

in which the quantity $2(m_c^* k_B T_c/2\pi\hbar^2)^{3/2}$ is referred to as the effective density of states (N_c). The Fermi–Dirac integral $F_{1/2}(\eta_c)$ can be calculated from Eq. (9) and in turn, the reduced Fermi level η_c provided that n_c and N_c (or T_c) are given. Once η_c is determined, the value of $F_\xi(\eta_c)$ of any order ξ can be obtained. The calculation of the Fermi–Dirac integrals and a numerical table covering integer orders from $\xi = -1$ to $\xi = 4$ and half-integer orders from $\xi = -3/2$ to $\xi = 7/2$ for the range of arguments $-4 \leqslant \eta_c \leqslant 10$ can be found in Ref. [13].

2.1. Rate equation for carrier pairs

For laser-generated plasmas, both types of the carriers basically move together. The Dember field, which develops because of charge separation, prohibits the carrier charge and current densities from becoming significantly different, respectively. Thus, one can assume

$$n_e = n_h = n, \quad \bar{j}_e = -\bar{j}_h \tag{10}$$

From the definition of the carrier pair current $\bar{J} = -\bar{j}_e/q = \bar{j}_h/q$ and Eq. (1), one obtains

$$\bar{J} = \frac{1}{q^2}\frac{\sigma_e\sigma_h}{\sigma_e+\sigma_h}\left[\nabla(\varphi_h - \varphi_e) + q(S_e - S_h)\right] \tag{11}$$

By taking the gradient on both sides of Eq. (9), utilizing the relationship $\mathrm{d}F_l(\eta_c)/\mathrm{d}\eta_c = F_{l-1}(\eta_c)$ [13], taking the gradient of η_c in Eq. (8), substituting the above results and Eq. (4) for S_c into Eq. (11) and regrouping, the following relationship is established:

$$\bar{J} = -D\left\{\begin{array}{l}\nabla n + \frac{n}{k_B T_e}\left[H_{-1/2}^{1/2}(\eta_e) + H_{-1/2}^{1/2}(\eta_h)\right]^{-1}\nabla E_g \\ \quad + \frac{n}{T_e}\left\{2\left[H_0^1(\eta_e) + H_0^1(\eta_h)\right]/\left[H_{-1/2}^{1/2}(\eta_e) + H_{-1/2}^{1/2}(\eta_h)\right] - \frac{3}{2}\right\}\nabla T_e\end{array}\right\} \tag{12}$$

where the band-gap energy $E_g = E_C - E_V$; the ambipolar diffusion coefficient is

$$D = \frac{k_B T_e}{q} \frac{\mu_e^0 \mu_h^0 H_{1/2}^0(\eta_e) H_{1/2}^0(\eta_h)}{\mu_e^0 H_{1/2}^0(\eta_e) + \mu_h^0 H_{1/2}^0(\eta_h)} \left[H_{-1/2}^{1/2}(\eta_e) + H_{-1/2}^{1/2}(\eta_h) \right] \tag{13}$$

The balance equation for the electron–hole pairs generated with a laser pulse is

$$\frac{\partial n}{\partial t} = \frac{\alpha I(\bar{x}, t)}{h\nu} + \frac{\beta I^2(\bar{x}, t)}{2h\nu} - \gamma n^3 + \theta n - \nabla \cdot \bar{J} \tag{14}$$

The terms on the right-hand side of Eq. (14) represent the carrier generation rates from the linear (one-photon) and nonlinear (two-photon) absorption, the Auger recombination, the impact ionization, and the loss due to the carrier current, respectively.

2.2. Rate equation for carrier energy

The ambipolar energy current is the sum of the carrier energy currents in electrons and holes, $\overline{W} = \bar{w}_e + \bar{w}_h$. Substitution of Eq. (5) for π_c, Eq. (8) for φ_c, and the relationship $\bar{J} = -\bar{j}_e/q = \bar{j}_h/q$ into $\overline{W}$ results in

$$\overline{W} = \left\{ E_g + 2k_B T_e \left[H_0^1(\eta_e) + H_0^1(\eta_h) \right] \right\} \bar{J} - (\kappa_e + \kappa_h) \nabla T_e \tag{15}$$

Eq. (15) indicates that the ambipolar energy current depends upon not only the carrier temperature gradient but also the carrier flow.

The total energy density (U) in the electron–hole pairs is the product of the carrier number density and the sum of the band-gap energy per unit volume and the kinetic energy

$$U = n \left\{ E_g + \frac{3}{2} k_B T_e \left[H_{1/2}^{3/2}(\eta_e) + H_{1/2}^{3/2}(\eta_h) \right] \right\} \tag{16}$$

The total energy balance equation for the electron–hole pairs is thus written as

$$\frac{\partial U}{\partial t} = (\alpha + \Theta n) I(\bar{x}, t) + \beta I^2(\bar{x}, t) - \nabla \cdot \overline{W} - \frac{C_{e\text{–}h}}{\tau_e}(T_e - T_l) \tag{17}$$

where Θn is the absorption of light by free carriers, and $C_{e\text{–}h} = \partial U / \partial T_e|_n$ is the heat capacity of electron–hole pairs. The first two terms on the right-hand side of Eq. (17) denote the volumetric laser heat source, and the last two terms are the rate of energy loss due to the ambipolar energy current and the rate of energy exchange between the carriers and the lattice respectively.

Substitution of Eq. (16) for U into Eq. (17) yields

$$\begin{aligned} C_{e\text{–}h} \frac{\partial T_e}{\partial t} = {} & (\alpha + \Theta n) I(\bar{x}, t) + \beta I^2(\bar{x}, t) - \nabla \cdot \overline{W} \\ & - \frac{C_{e\text{–}h}}{\tau_e}(T_e - T_l) \\ & - \frac{\partial n}{\partial t} \left\{ E_g + \frac{3}{2} k_B T_e \left[H_{1/2}^{3/2}(\eta_e) + H_{1/2}^{3/2}(\eta_h) \right] \right\} \\ & - n \left(\frac{\partial E_g}{\partial n} \frac{\partial n}{\partial t} + \frac{\partial E_g}{\partial T_l} \frac{\partial T_l}{\partial t} \right) \end{aligned} \tag{18}$$

with

$$\begin{aligned} C_{e\text{–}h} = {} & \frac{3}{2} n k_B \Big\{ H_{1/2}^{3/2}(\eta_e) + H_{1/2}^{3/2}(\eta_h) \\ & - \eta_e \left[1 - H_{1/2}^{3/2}(\eta_e) H_{1/2}^{-1/2}(\eta_e) \right] \\ & - \eta_h \left[1 - H_{1/2}^{3/2}(\eta_h) H_{1/2}^{-1/2}(\eta_h) \right] \Big\} + n \frac{\partial E_g}{\partial T_e} \end{aligned} \tag{19}$$

The last two terms on the right-hand side of the carrier energy balance equation (18) are the rate of change of the carrier energy density due to the changes of the carrier density and the band-gap energy, respectively.

2.3. Rate equation for lattice energy

For semiconductor materials the lattice thermal conductivity is comparable with the bulk value; therefore, thermal transfer in the lattice should be incorporated into the heat conduction equation [14]. Thus,

$$C_l \frac{\partial T_l}{\partial t} = \nabla \cdot (k_l \nabla T_l) + \frac{C_{e\text{–}h}}{\tau_e}(T_e - T_l) \tag{20}$$

The three rate equations for the electron–hole pair density, the carrier temperature, and the lattice temperature, (14), (18) and (20), together with the constitutive equations for the carrier pair current and the ambipolar energy current, (12) and (15), compose the complete self-consistent model for ultrafast transport dynamics in semiconductors subjected to short-pulse laser heating. The pair density, the carrier and lattice temperature, and the carrier pair and ambipolar energy current can be solved with proper initial and boundary conditions.

It is noted that Eq. (14) reduces to a carrier density model when the divergence of carrier current ($\nabla \cdot \bar{J}$) is neglected. Hence, the carrier density can be solved with this simple model as long as the four material properties α, β, γ and θ are assumed to be temperature independent. The capability of both the self-consistent model and the carrier density model will be investigated and compared later.

2.4. Non-degenerate systems of electrons

When the quasi-Fermi level $\varphi_e(\varphi_h)$ is considerably lower than E_C (higher than E_V), the reduced Fermi level

$\eta_e(\eta_h)$ is large and negative. Consequently, all the Fermi–Dirac integrals are approximately equal to $\exp(\eta_e)$ [or $\exp(\eta_h)$]. This corresponds to the assumption of Maxwell–Boltzmann distribution, $n_e = N_e \exp(\eta_e)$, which is also referred to the non-degenerate system. Since $H^{\xi}_{\zeta}(\eta_c) \to 1$ for all ξ and ζ, the equations for the carrier pair current, the total ambipolar energy current, and the carrier energy density can respectively be simplified from Eqs. (12), (15) and (18) to

$$\bar{J} = -D\left(\nabla n + \frac{n}{2k_B T_e}\nabla E_g + \frac{n}{2T_e}\nabla T_e\right) \tag{21}$$

$$\overline{W} = (E_g + 4k_B T_e)\bar{J} - (\kappa_e + \kappa_h)\nabla T_e \tag{22}$$

$$C_{e\text{-}h}\frac{\partial T_e}{\partial t} = (\alpha + \Theta n)I(\bar{x}, t) + \beta I^2(\bar{x}, t) - \nabla \cdot \overline{W} - \frac{C_{e\text{-}h}}{\tau_e}(T_e - T_l) - \frac{\partial n}{\partial t}(E_g + 3k_B T_e) - n\left(\frac{\partial E_g}{\partial T_l}\frac{\partial T_l}{\partial t} + \frac{\partial E_g}{\partial n}\frac{\partial n}{\partial t}\right) \tag{23}$$

In addition, the ambipolar diffusivity, Eq. (13), reduces to

$$D = D_0 = \frac{2k_B T_e}{q}\frac{\mu_e^0 \mu_h^0}{\mu_e^0 + \mu_h^0} \tag{24}$$

and the electron–hole pair heat capacity

$$C_{e\text{-}h} = 3nk_B + n\frac{\partial E_g}{\partial T_e} \tag{25}$$

3. Laser intensity

The laser intensity $I(\bar{r}, t)$ in the first two terms on the right-hand side of Eqs. (14) and (18) needs to be described. For a volume-absorbing material, the laser attenuation in the direction of propagation (z) can be obtained by solving the propagation loss due to the one- and two-photon absorption and the free-carrier absorption [15]

$$\frac{\partial I}{\partial z} = -(\alpha + \Theta n)I - \beta I^2 \tag{26}$$

For the constant values of α, Θn and β, a closed-form solution of the laser intensity is derived by integrating the differential equation (26)

$$I(\bar{x}, t) = \frac{(\alpha + \Theta n)I_0 e^{-(\alpha+\Theta n)z}}{(\alpha + \Theta n) + \beta I_0[1 - e^{1-(\alpha+\Theta n)z}]} \tag{27}$$

where I_0 is the transmitted laser intensity at the beam incident surface ($z = 0$). Neglecting the effect of the free-carrier absorption reduces Eq. (27) to that derived by Zhang and Chen [16]. If any of the above three properties is temperature dependent or the carrier density varies with location, the laser intensity must be solved numerically with the coupled rate equations.

The optical penetration depth (δ) is defined as the distance z at which I/I_0 is equal to e^{-1}. It is obtained from Eq. (27)

$$\delta = \frac{1}{\alpha + \Theta n}\ln\left[\frac{e(\alpha + \Theta n) + \beta I_0}{\alpha + \Theta n + \beta I_0}\right] \tag{28}$$

The penetration depth $1/\alpha$ for single-photon absorption can be retrieved from Eq. (28) by letting $\beta = \Theta = 0$.

When a laser beam is gaussian in both time and space, the transmitted laser intensity at the incident surface is expressed in the form

$$I_0(r, t) = \sqrt{\frac{\omega}{\pi}}\frac{(1 - R)\Phi}{\pi b^2 t_p} e^{-(r/b)^2} e^{-\omega[(t-3t_p)/t_p]^2} \tag{29}$$

The pulse duration (t_p) is defined as the full width at the half maximum. It is assumed in this paper that the lasing starts at $t = 0$, reaches the maximum power at $t = 3t_p$, and ends at $t = 6t_p$. For ultrashort laser material interactions, a one-dimensional (1D) heating problem is often analyzed since the heating spot size is much larger than the depth of the thermally affected zone [17]. Letting $\phi = \Phi/\pi b^2$ and $b \to \infty$ in Eq. (29) leads to the 1D form of the laser intensity

$$I_0(t) = \sqrt{\frac{\omega}{\pi}}\frac{(1 - R)\phi}{t_p} e^{-\omega[(t-t_m)/t_p]^2} \tag{30}$$

4. Numerical results and discussion

The 1D version of the three governing equations (14), (18) and (20) together with the constitutive equations (12) and (15) and the following initial and boundary conditions are solved with a finite difference method:

$$n(z, 0) = 10^{12}\,\text{cm}^{-3}, \quad T_e(z, 0) = T_l(z, 0) = 300\ \text{K} \tag{31}$$

$$J(z, t) = 0, \quad W(z, t) = 0, \quad q_l(z, t) = 0 \text{ at } z = 0, L \tag{32}$$

The finite difference grid mesh is sketched in Fig. 1. The spatial derivatives of n, T_e, T_l, J, W, $Q_l(= -k_l\partial T_l/\partial z)$,

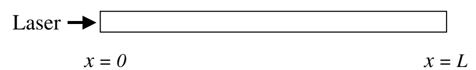

(a): 1D laser heating

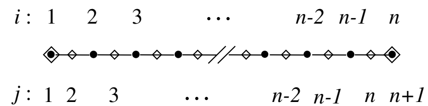

(b): Finite difference grid points

• Grid points for n, T_e and T_l ($i = 1, 2, \ldots, n$)

◊ Grid points for J, W, Q_l, and E_g ($j = 1, 2, \ldots, n+1$)

Fig. 1. Finite difference grid mesh.

Table 1
Model parameters

Properties	Silicon	Germanium
K_l (W/cm K)	$1585T_l^{-1.23}$	$675T_l^{-1.23}$
C_l (J/cm^3)	$1.978 + 3.54 \times 10^{-4}T_l - 3.68T_l^{-2}$	$1.7 \cdot (1 + T_l/6000)$
K_e (eV/sÅ K)	$-3.47 \times 10^8 + 4.45 \times 10^6 T_e$	$-3.58 \times 10^9 + 6.49 \times 10^6 T_e$
τ_e (fs)	$240 \cdot (1 + n/6.0 \times 10^{20}\,\mathrm{cm}^{-3})$	$300 \cdot (T_l/T_{rm})^{-2.5}$
γ (cm^6/s)	3.8×10^{-31}	2.0×10^{-31}
θ (s^{-1})	$3.6 \times 10^{10} \exp(-1.5E_g/k_B T_e)$	
D_0 (cm^2/s)	$18 \cdot (T_{rm}/T_l)$	$65 \cdot (T_l/T_{rm})^{-1.5}$
E_g (eV)	$1.16 - 7.02 \times 10^{-4}T_l^2/(T_l + 1108) - 1.5 \times 10^{-8}n^{1/3}$	$0.803 - 3.9 \times 10^{-4}T_l$
R	$0.37 + 5 \times 10^{-5} \cdot (T_l - T_{rm})$	0.45
α (cm^{-1})	$5.02 \times 10^3 \exp(T_l/430)$	$6.0 \times 10^3 \exp(T_l/430)$
β (cm/GW)	2.0	
Θ (cm^2)	$5.1 \times 10^{-18} \cdot (T_l/T_{rm})$	
m_e^*	0.33	0.22

and E_g at the interior points are approximated with the central difference, and those at the boundary are evaluated with the first-order approximation. A forward difference scheme is employed to advance$n$, T_e and T_l. Two materials, Si and Ge, irradiated with a 775-nm laser are investigated. Their material properties used in the numerical analysis are listed in Table 1 [12,18–20]. For both materials the sample thickness is set to be 20 μm, for which it is large compared to the optical penetration length and the maximum carrier diffusion distance. A total of 61 equally-spaced grid points for n, T_e and T_l is found to be sufficiently fine to resolve the problem. In fact, the result obtained from a model consisting of 21 points was within in 1.0% difference from the 61-point model. The time step is set at 0.5×10^{-19} s for the self-consistent model and 1.0×10^{-17} s for the carrier density model.

Fig. 2 shows the time history of the carrier density and temperature and the lattice temperature at the incident surface ($z = 0$) for a silicon sample irradiated by a 500-fs laser pulse of $\phi = 0.005$ J/cm^2. Attention is paid to the peak of the carrier temperature. It occurs at about $t = 0.68$ ps, earlier than the occurrence of the laser peak power ($t = 1.5$ ps). On the other hand, the peak of the carrier density takes place at a much later time, about 2.21 ps. When the peak carrier temperature occurs, the laser intensity is only about 0.06% of the maximum. Now that the laser energy deposited into the material by the time instance is so small compared to the total absorbed energy, how can the carrier temperature reach the maximum at this early time? The reason is as follows. Five sources, as given by Eq. (18), are competing for the energy change ($C_{e-h}\partial T_e \partial t$) that leads to elevated carrier temperature. The numerical result shows that before the peak carrier temperature, the absorbed laser energy and the change of the carrier energy density due to the change of the carrier density are predominating over the other three. The resulting rate of the net energy change is positive although it is small. Of consequence, a very small amount of the electron–hole pairs are created during this early time. This, according to Eq. (19), leads to a small carrier heat capacity and thereby a rapid, noticeable rise in the carrier temperature. As the time increases, the carrier density increases drastically because a much more laser energy has been absorbing. As a result of the large number of the carriers generated, the energy change due to the rapid change of the carrier density (the last second term on the right-hand side of Eq. (18)) becomes pronounced, and so does the energy loss due to the thermal transfer from the carriers to the lattice. The change makes the rate of the net energy change unable to remain positive at some point and thereafter even though considerably large laser energy is absorbed. This explains why the carrier temperature continues falling after it reaches the peak. The numerical result also shows that the carrier diffusion and the impact ionization both have very little impact on the creation of electron–hole carriers. In fact, one-pho-

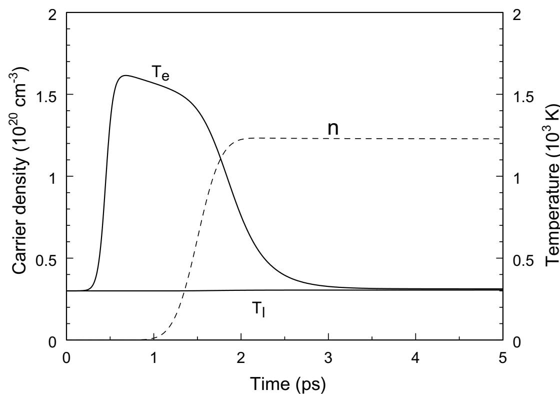

Fig. 2. Time evolution of carrier density (n), carrier temperature (T_e), and lattice temperature (T_l) at the front surface ($z = 0$) of a 20-μm silicon sample heated by a 500-fs laser pulse at fluence $\phi = 0.005$ J/cm^2.

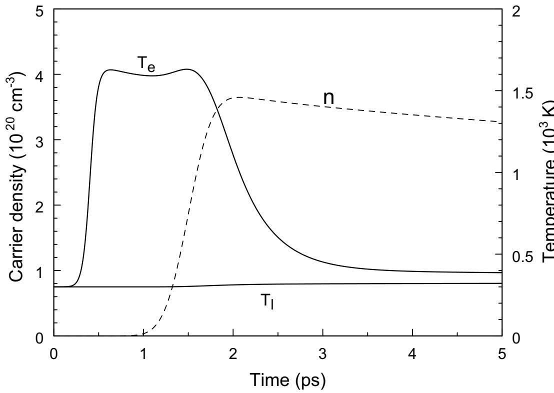

Fig. 3. Time evolution of carrier density (n), carrier temperature (T_e), and lattice temperature (T_l) at the front surface ($z = 0$) of a 20-μm silicon sample heated by a 500-fs laser pulse at fluence $\phi = 0.015\,\mathrm{J/cm^2}$.

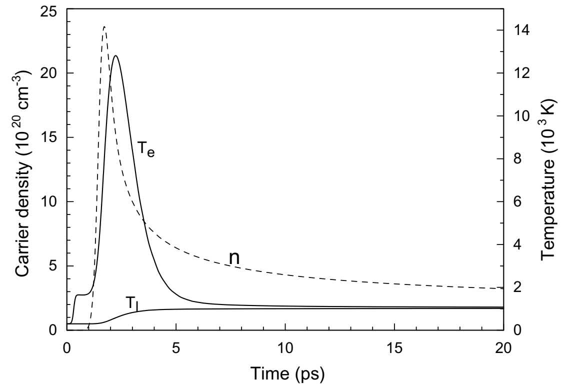

Fig. 4. Time evolution of carrier density (n), carrier temperature (T_e), and lattice temperature (T_l) at the front surface ($z = 0$) of a 20-μm silicon sample heated by a 500-fs laser pulse at fluence $\phi = 0.15\,\mathrm{J/cm^2}$.

ton absorption and the Auger recombination are the two crucial factors that alter the carrier density.

Two peaks structure of the carrier temperature is shown in Fig. 3, where the results are computed with $\phi = 0.015\,\mathrm{J/cm^2}$. The first peak carrier temperature is 1627 K at about $t = 0.63$ ps, and the second peak is 1631 K at about 1.48 ps. Two peaks both occur before the carrier density reaches the maximum. The first peak carrier temperature is slightly higher than that of the previous case (1615 K) although the laser power is two times higher. Due to the fact that the Auger electron–hole recombination rate is proportional to the carrier density cubed, the reduction rate in the carrier density should be different between the two cases. This is confirmed by comparing the declining slopes of n in Figs. 2 and 3. It is evident also, by comparing the carrier and lattice temperature in Figs. 2 and 3, that it takes a longer time for a high fluence to establish the thermal equilibrium than for a low fluence.

Fig. 4 displays the time evolution of n, T_e and T_l at $z = 0$ for $\phi = 0.15\,\mathrm{J/cm^2}$. Like the previous two relatively low fluence cases, T_e rises rapidly and reaches its peak in the very beginning. After a slight decrease, however, T_e soars to a much higher peak that occurs beyond the peak carrier density.

As mentioned previously, one-photon absorption and the Auger recombination are the two crucial factors that alter the carrier density. Their effects are presented in Fig. 5, where the results are calculated at the incident surface of a Si sample irradiated by the 500-fs lasers of different fluences. The one-photon absorption coefficient (α) used in this paper is lattice temperature dependent, $5.02 \times 10^3 \exp(T_l/430)\,\mathrm{cm^{-1}}$, while the Auger recombination coefficient (γ) is constant, $3.8 \times 10^{-31}\,\mathrm{cm^6/s}$. For ease of explanation, these values are referred to as case (a). The other cases considered are: (b) $\alpha = 5.02 \times 10^3 \exp(T_l/430)\,\mathrm{cm^{-1}}$ and $\gamma = 0$ and (c) $\alpha = 1.004 \times 10^4\,\mathrm{cm^{-1}}$ and $\gamma = 0$. The constant α in case (c) is the value at room temperature. It is seen in Fig. 5 that the carrier density computed from case (c) is nearly linearly proportional to the laser fluence. For the laser pulses studied here, it generally takes about 2 ps (more or less depending the laser fluence) for the carrier density to reach the maximum. At this moment, the lattice is already heated up by the hot carriers. For the $0.15\,\mathrm{J/cm^2}$ laser pulse, for example, the lattice temperature is 377 K at about $t = 1.72$ ps, the time when the carrier density reaches the maximum (Fig. 4). At this temperature α would increase by about 20%. Since the optical penetration depth basically is inversely proportional to the one-photon absorption coefficient, a larger portion of the laser

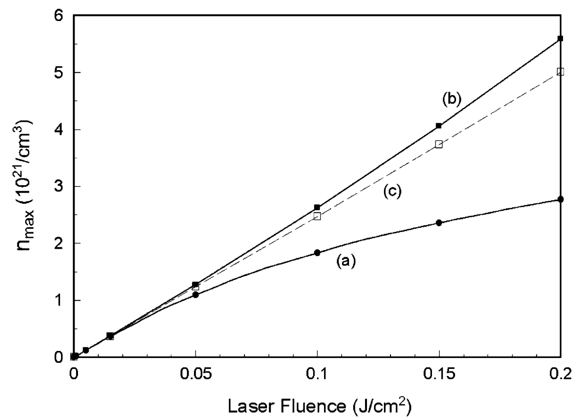

Fig. 5. Maximum number density of carriers at the incident surface of Si generated by a 500-fs laser pulse: (a) $\alpha = 5.02 \times 10^3 \exp(T_l/430)\,\mathrm{cm^{-1}}$ and $\gamma = 3.8 \times 10^{-31}\,\mathrm{cm^6/s}$, (b) $\alpha = 5.02 \times 10^3 \exp(T_l/430)\,\mathrm{cm^{-1}}$ and $\gamma = 0$, and (c) $\alpha = 1.004 \times 10^4\,\mathrm{cm^{-1}}$ and $\gamma = 0$.

energy is absorbed and consequently more electron–hole carriers are created near the incident surface. Comparing the results (b) and (c) in Fig. 5 indicates the effect of the one-photon absorption on the carrier density. When the Auger recombination effect is included, the carrier density should decrease due to the n^3 decaying rate. The result (a) in Fig. 5 shows the reduction of the carrier density caused by the Auger recombination.

Non-thermal melting is assumed to occur when the maximum carrier density is equal to the critical value. It has been an open question at which electron density the ultrafast disordering of the crystal happens, although the range of 10^{21}–$10^{22}\,\mathrm{cm}^{-3}$ is generally believed. In this work, the critical electron density for the initiation of lattice disordering in Si is set at $2.74 \times 10^{21}\,\mathrm{cm}^{-3}$ for the self-consistent model and $2.60 \times 10^{21}\,\mathrm{cm}^{-3}$ for the carrier density model so that the computed damage thresholds are the same and match the experimental data for the 500-fs pulse case. Fig. 6 compares the theoretical damage fluence thresholds with the measured value [9,21] for Si. It appears that the self-consistent model agrees fairly well with the experimental data; on the other hand, the carrier density model is only in good agreement for $t_p < 1$ ps. The dimensionless time (t_f/t_p) and the lattice temperature at the onset of damage are given in Fig. 7 as a function of the laser pulse length. For the pulse durations investigated, non-thermal melting always initiates in the time interval of $3t_p$–$4t_p$, sometime after the lasers pass their peak power. The lattice temperature at the onset of damage increases with the laser pulse length, especially for picosecond pulses. The lattice temperature before the onset of damage plays an important role in the model prediction of the damage threshold. For sub-picosecond laser heating, the change of one-photon absorption is minor because the lattice basically remains thermally undisturbed (Fig. 7). Therefore, as illustrated in Fig. 6, there is an insignificant difference of the damage threshold between the two models. The discrepancy, however, becomes pronounced for picosecond pulses due to the fact that a much greater one-photon absorption that results from the significant lattice temperature rise is used in the self-consistent model.

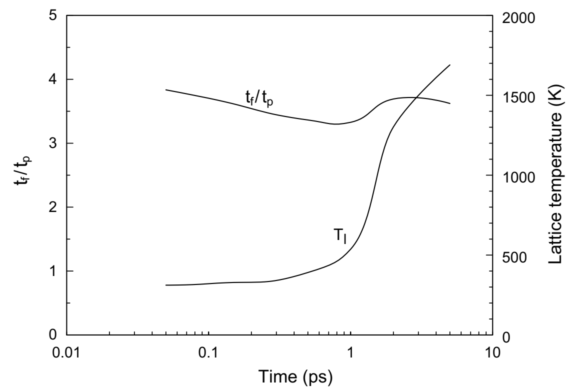

Fig. 7. Dimensionless time and lattice temperature at the onset of damage in Si.

It is noted here that for the 5-ps laser case the computed lattice temperature reaches the normal (slow heating) melting point at about $t = 18.03$ ps, slightly before the maximum carrier density reaches the critical value, at $t = 18.11$ ps. It is believed that for such an extremely short laser heating, material would undergo an ultrafast superheating process and the resulting melting point could be well beyond the normal one. To improve the damage assessment for picosecond pulses, more accurate material properties, particularly for the one-photon absorption and Auger recombination, and the kinetics of an ultrafast superheating process are needed. Further investigation on these issues is suggested.

Fig. 8 compares the theoretical non-thermal melting thresholds with the measurement [9] for Ge semiconduc-

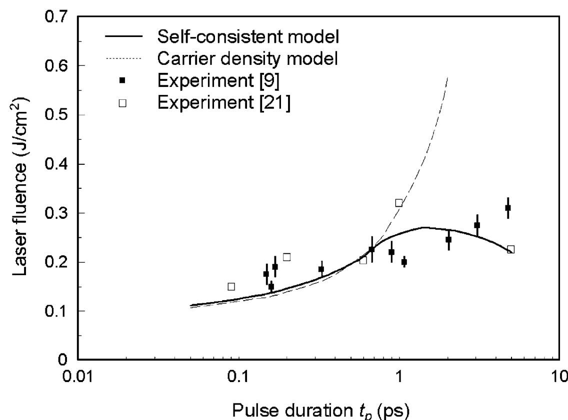

Fig. 6. Theoretical and experimental damage threshold of Si.

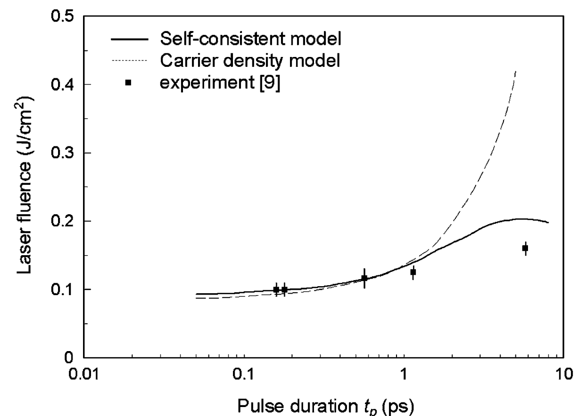

Fig. 8. Theoretical and experimental damage threshold of Ge.

tor. In this case the critical electron density is set at $2.32 \times 10^{21}\,\mathrm{cm}^{-3}$ for the self-consistent model and $2.15 \times 10^{21}\,\mathrm{cm}^{-3}$ for the carrier density model. Again, the self-consistent model matches fairly well with the experimental data while the carrier density model is only in good correlation for $t_p < 1\,\mathrm{ps}$.

It should be noted here that in the present numerical study the reduced Fermi levels (η_c) are found to be <-10. At those values, all the Fermi–Dirac integrals are approximately equal to $\exp(\eta_c)$ and thus $H_\zeta^\xi(\eta_c) \to 1$. This suggests that the equations given in Section 2.4 for the non-degenerate system be sufficient for the investigation of non-thermal melting.

5. Conclusions

A complete self-consistent model for transport dynamics in semiconductors caused by ultrashort-pulse laser heating is presented based on the relaxation-time approximation of the Boltzmann equation. The carrier–lattice nonequilibrium interactions are simulated with a finite difference method to obtain the temporal and spatial evolution of the carrier density and temperature as well as the lattice temperature. Generally speaking, the maximum electron–hole carrier density occurs after the laser passes its peak power. For low laser fluences, there is only one peak of the carrier temperature. It occurs at a very early time due to the low carrier heat capacity. For high laser fluences, on the other hand, two peak structures of the carrier temperature can be established. The self-consistent model and the carrier density model are compared for their capability of evaluating the damage threshold. It is found that the self-consistent model correlates fairly well with the experimental data, while the carrier density model is only in good agreement for $t_p < 1\,\mathrm{ps}$. To improve the damage prediction of the self-consistent model for picosecond pulses, accurate temperature-dependent material properties, particularly for the one-photon absorption and Auger recombination, and the kinetics of an ultrafast superheating process are needed. Further investigation on these issues is suggested.

References

[1] S.M. Metev, V.P. Veiko, Laser-Assisted Microtechnology, Springer-Verlag, Berlin, 1994, pp. 109–121.
[2] H.M. van Driel, Physics of pulsed laser processing of semiconductors, in: R.R. Alfano (Ed.), Semiconductors Probed by Ultrafast Laser Spectroscopy, vol. II, Academic Press, Orlando, FL, 1984, pp. 57–94.
[3] C.V. Shank, R. Yen, C. Hirlimann, Time-resolved reflectivity measurements of femtosecond-optical pulse-induced phase transitions in silicon, Phys. Rev. Lett. 50 (1983) 454–457.
[4] H.W.K. Tom, G.D. Aumiller, C.H. Brito-Cruz, Time-resolved study of laser-induced disorder of Si surfaces, Phys. Rev. Lett. 60 (1988) 1438–1441.
[5] S.V. Govorkov, T. Schröder, I.L. Shumay, P. Heist, Transient gratings and second-harmonic probing of the phase transformation of a GaAs surface under femtosecond laser irradiation, Phys. Rev. B 46 (1992) 6864–6868.
[6] K. Sokolowsi-Tinten, D. von der Linde, Generation of dense electron–hole plasmas in silicon, Phys. Rev. B 61 (2000) 2643–2650.
[7] A. Rousse, C. Rischel, S. Fourmanux, I. Uschmann, S. Sebban, G. Grillon, Non-thermal melting in semiconductors measured at femtosecond resolution, Nature 410 (2001) 65–68.
[8] J.A. Van Vechten, R. Tsu, F.W. Saris, Nonthermal pulsed laser annealing of Si: plasma annealing, Phys. Lett. 74A (1979) 422–426.
[9] P. Allenspacher, B. Hüttner, W. Riede, Ultrashort pulse damage of Si and Ge semiconductors, SPIE 4932 (2003) 358–365.
[10] K. Sokolowski-Tinten, D. von der Linde, Generation of dense electron–hole plasmas in silicon, Phys. Rev. B 61 (2000) 2643–2650.
[11] J.R. Drabble, H.J. Goldsmid, Thermal Conduction in Semiconductors, Pergamon Press, Oxford, 1961.
[12] H.M. van Driel, Kinetics of high-density plasmas generated in Si by 1.06- and 0.53-μm picosecond laser pulses, Phys. Rev. B 35 (1987) 8166–8176.
[13] J.S. Blakemore, Semiconductor Statistics, Pergamon Press, Oxford, 1962.
[14] J.K. Chen, J.E. Beraun, C.L. Tham, Ultrafast thermoelasticity for short-pulse laser heating, Int. J. Eng. Sci. 42 (2004) 793–807.
[15] T.F. Boggess, K.M. Bohnert, K. Mansour, S.C. Moss, I.W. Boyd, A.L. Smirl, Simultaneous measurement of the two-photon coefficient and free-carrier cross section above the bandgap of crystalline silicon, IEEE J. Quant. Electron. QE-22 (1986) 360–368.
[16] Z.M. Zhang, D.H. Chen, Thermal analysis of multiphoton absorption at 193 nm in volume-absorbing glass, ASME J. Heat Transfer 124 (2002) 391–394.
[17] J.K. Chen, W.P. Latham, J.E. Beraun, Axisymmetric modeling of femtosecond pulse laser heating on metal films, Numer. Heat Transfer B 42 (2002) 1–17.
[18] M.I. Gallant, H.M. van Driel, Infrared reflectivity probing of thermal and spatial properties of laser-generated carriers in germanium, Phys. Rev. B 26 (1982) 2133–2146.
[19] D. Agassi, Phenomenological model for picosecond-pulse laser annealing of semiconductors, J. Appl. Phys. 55 (1984) 4376–4383.
[20] T. Sjodin, H. Petek, H.L. Dai, Ultrafast carrier dynamics in silicon: a two-color transient reflection grating study on a (111) surface, Phys. Rev. Lett. 81 (1998) 5664–5667.
[21] P.P. Pronko, P.A. VanRompay, C. Horvath, F. Loesel, T. Juhasz, X. Liu, G. Mourou, Avalanche ionization and dielectric breakdown in silicon with Ultrafast laser pulses, Phys. Rev. B 58 (1998) 2387–2390.